5.
CASTOR LEAF-SHAPED QUASI-SELF-COMPLEMENTARY ANTENNA AS AN ELEMENT FOR MIMO APPLICATION WITH BAND-REJECTION CHARACTERISTICS

5.1 Introduction

Owing to the advancement in modern high speed wireless communication systems, the need for design and development of compact and broadband multiple-input-multiple-output (MIMO) antennas has arisen in recent years. MIMO communication system using broadband antenna elements meets the requirement of high data transmission/reception rate with minimal multipath fading in short range communication. The broadband antennas having planar printed geometry are advantageous to be used as elements of a MIMO antenna system due to their inherent properties such as their compact size, simple structure, low cost manufacturing and easy mountability on planar surfaces. In recent years, various planar antennas have been designed and reported for broadband applications. Some of the planar antennas with natural shapes have specially designed curved boundaries providing broad bandwidth and compact antenna size as discussed in chapter 1 and flower-shaped planar monopole antenna (PMA) investigated in chapter 4. It is also discussed in Chapter 2: Literature Review that the MIMO antenna system designed using PMAs needs isolation structure between orthogonally arranged antenna elements which increases the size of the antenna system. Among various antennas, self-complementary antenna (SCA) first discovered by Mushiake [Mushiake (1992)] is a well known broadband antenna and can become a good candidate to act as MIMO antenna element. An SCA can ideally provide infinite impedance bandwidth when designed on infinite large ground plane. Its self-complementary structure is designed in such a way that it's input impedance (= 188.5 Ω) becomes constant regardless of frequencies used. But the practical antenna has limited bandwidth because of finite antenna size and requirement of providing impedance matching circuit. However, in order to achieve desired bandwidth and integration of antenna with 50 Ω coaxial cable, an appropriate impedance matching circuit is

required between the antenna and coaxial cable for impedance transformation from 188.5 to 50 Ω. These issues are resolved with the development of a quasi-self-complementary antenna (QSCA) [Guo *et al.* (2008)] having compact size and in-built impedance matching circuit. The development of QSCA has grown the family of SCAs to a higher level. In references [Guo *et al.* (2009), Huang *et al.* (2012)a and b, and Lin *et al.* (2013)], QSCAs are described in which the conducting patch and complementary slot of antenna have been designed on opposite sides of substrate and impedance matching is achieved using a microstrip line feed. The single-sided QSCA [Lin (2012) and Guo *et al.* (2010)], which has both the patch and its complementary slot on same side of substrate, is fed using CPW. The supporting ground plane acts as impedance matching circuit. Due to its inherent properties including its compact size, planar self-complementary geometry and broad bandwidth, QSCA can be a potential candidate for design of a broadband MIMO antenna. In references [Liu *et al.* (2014)a and b], microstrip line-fed half-circular self-complementary antenna elements designed on both sides of substrate have been reported for UWB applications. Two rectangular slots on ground plane have been reported to enhance isolation and tapered microstrip line has been used for improvement of impedance matching [Liu *et al.* (2014)a]. Further, high isolation is achieved without the use of any extra isolation technique and impedance matching is improved using impedance transformer section [Liu *et al.* (2014)b]. The UWB spectrum interferes with existing narrowband communication spectrums such as worldwide interoperability for microwave access WiMAX, (3.3−3.8 GHz) and wireless local area network WLAN, (5.15−5.825 GHz). These overlapping frequency bands must be rejected in order to avoid interference from these frequency bands. The single WLAN band rejection is achieved using slit or slot loaded on the patch [Zhu *et al.* (2016) and Gao *et al.* (2014)]. In reference [Li *et al.* (2013)], a metal strip and an open slot have been used for dual band rejection in MIMO antenna. To the best of authors' knowledge, single-sided QSCA with multiple band-rejection characteristics is not reported in the literature for broadband MIMO applications.

In this chapter, a broadband castor leaf-shaped quasi-self-complementary antenna (QSCA) is proposed. Initially, the design and performance comparison of two castor leaf-shaped QSCAs having sharp and smooth corners are presented. The geometry of the QSCA is inspired by naturally available castor leaf, which has multiple segments of increasing size. These multiple segments can resonate at multiple frequencies and provide broad bandwidth. Finally, MIMO antenna using two smooth-corner castor leaf-shaped QSCAs, which are mirror-images of each other, is described in which no extra isolation structure is used. The MIMO antenna is designed to cover wide frequency range including UWB and Bluetooth spectrums. The interfering WiMAX and WLAN narrowband spectrums are rejected, respectively, with the help of a slit and a hexagonal split ring slot (HSRS) loaded on each patch of the antenna. Each QSCA element is fed using 50 Ω coplanar waveguide (CPW), which allows the design of whole antenna on same side of substrate. The single-sided antenna is easy to fabricate and integrate with other planar devices than double-sided antenna. The simulation studies for input characteristics, radiation pattern and envelope correlation coefficient (ECC) of the proposed antenna were carried out using Computer Simulation Technology Microwave Studio (CST MWS) software. Further, the simulation results of the MIMO antennas without and with WiMAX and WLAN bands-rejection capability are compared with corresponding experimental results.

5.2 Design and Configurations of Castor Leaf-shaped QSCA

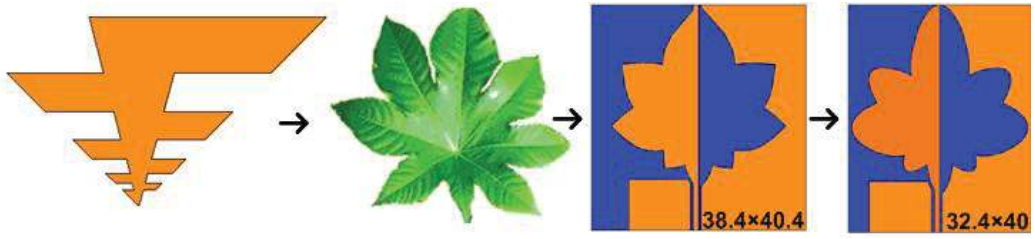

Figure 5.1: Geometries of (a) trapezoidal toothed log-periodic antenna, (b) castor leaf, (c) castor leaf-shaped QSCA with sharp corners, and (d) castor leaf-shaped QSCA with smooth corners.

The geometry of proposed antenna element is inspired by naturally available castor leaf having multiple segments of increasing size around its boundary as shown in Figure 5.1(b). These multiple segments may resonate at different frequencies. The multiple resonances due to the segments of the proposed antenna element's geometry providing broad bandwidth are similar to different resonant frequencies obtained due to differing teeth sizes of trapezoidal toothed log-periodic antenna (TTLPA) shown in Figure 5.1(a). With this basic idea, castor leaf-shaped antenna in self-complementary configuration was designed on FR4 substrate having thickness of 0.8 mm and relative permittivity of 4.4. Figure 5.1(c) shows the geometry of QSCA having sharp corners in which its dimensional details are not given while Figure 5.2(a) shows the geometry depicting its dimensional parameters also. The sharp outer corners of each segment of QSCA were modified to smooth corners, which make the antenna compact in size with same lower cutoff frequency. Figure 5.1(d) shows the geometry of QSCA having smooth corners in which its dimensional details are not given while Figure 5.2(b) shows the geometry depicting its dimensional parameters also.

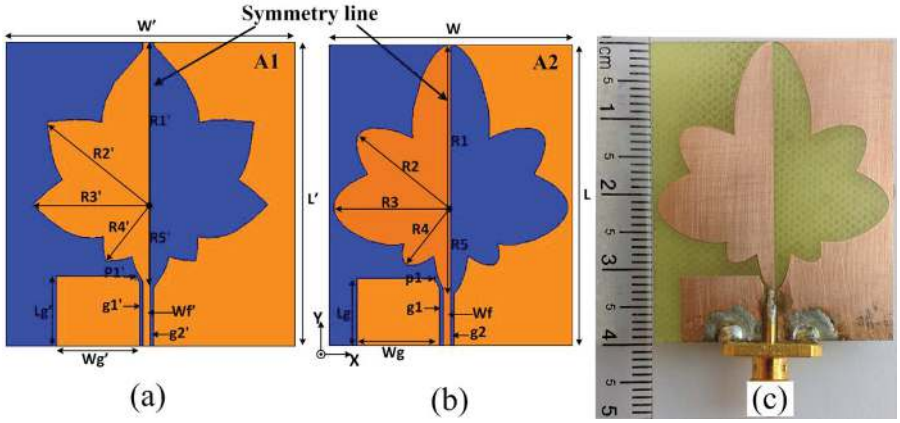

Figure 5.2: Geometry of the proposed single element QSCA having (a) sharp corners designated as A1, (b) smooth corners designated as A2, (c) the prototype having smooth corners.

The prototype of QSCA having smooth corners is shown in Figure 5.2(c). Each antenna geometry is split up into two symmetrical portions by cutting it along symmetry line. Half castor leaf-shaped radiating patch is attached to central

strip of 50 Ω CPW and its complementary slot is designed opposite to symmetry line. The segments of each type of QSCA element are designed using spline curves. The rectangular ground plane having an arc-shaped slit (near central strip of CPW) acts as the in-built matching circuit. The optimized dimensions of each type of antenna element shown in Figure 5.2 are listed in Table 5.1.

Table 5.1: Design parameters of QSCAs

Parameter		**Value (mm)**		**Parameter**		**Value (mm)**	
A1	**A2**	**A1**	**A2**	**A1**	**A2**	**A1**	**A2**
W'	W	38.4	32.4	R1'	R1	21.6	21.6
L'	L	40.4	40	R2'	R2	15.6	15.6
Wg'	Wg	11	11	R3'	R3	15.6	15.6
Lg'	Lg	9.3	9.3	R4'	R4	9.6	9.6
Wf'	Wf	1	1	R5'	R5	11.6	11.6
g1'	g1	0.5	0.4	p1'	p1	2	1.9
g2'	g2	0.4	0.4				

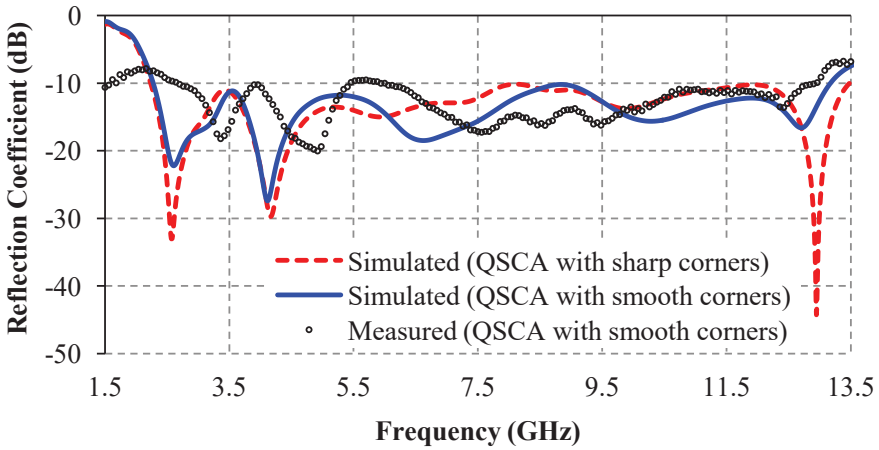

Figure 5.3: Reflection coefficient-frequency characteristics of single element QSCA having smooth/sharp corners.

Figure 5.3 shows the variations of simulated and experimental reflection coefficient-frequency characteristics of QSCA having smooth corners along with simulated reflection coefficient-frequency characteristic of the QSCA having sharp corners. It is observed from Figures 5.2, 5.3, and Table 5.1 that the QSCA having smooth corners is smaller in size as compared to the QSCA having sharp corners. Further, the former antenna element provides nearly the same -10 dB reflection coefficient bandwidth and identical lower cutoff frequency as the latter

element. In addition, it can be seen from Figure 5.3 that simulated reflection coefficient-frequency characteristic of the smooth corner QSCA element is nearly in agreement with the corresponding experimental characteristic. The proposed antenna element with smooth corners provides simulated $S_{11} \leq$ -10 dB for the broad frequency range of 2.2−13.1 GHz (bandwidth = 5.95:1 whereas its experimental -10 dB reflection coefficient bandwidth is found to be 5:1 (2.2−13.0 GHz) The slight deviation in simulated and experimental characteristics of QSCA element may be due to fabrication and measurement errors.

5.3 Design of two-element MIMO antenna

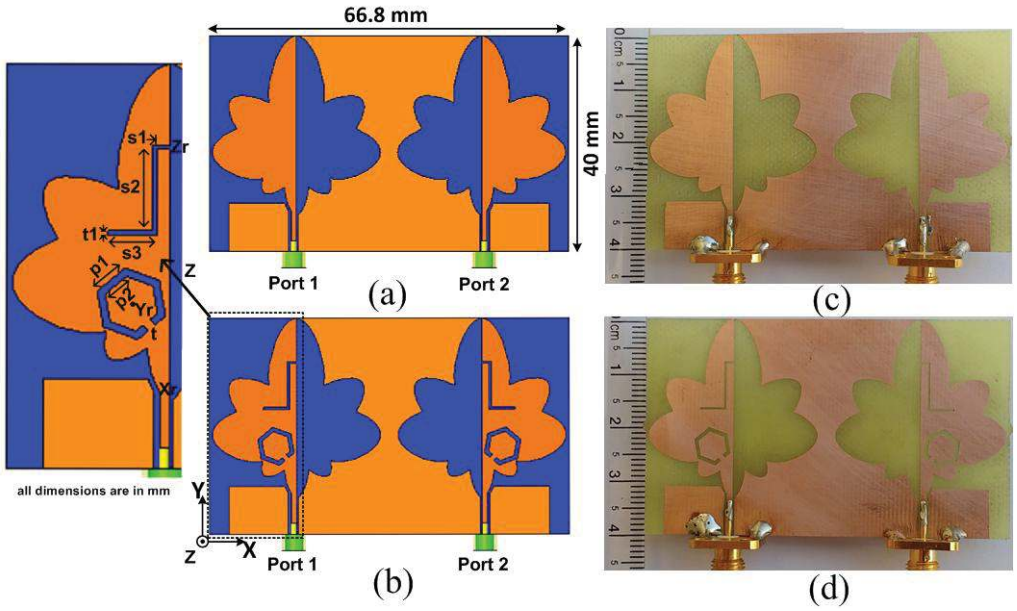

Figure 5.4: Geometry of the proposed two element MIMO antenna (a) without resonators and (b) with resonators; Prototype of the proposed antenna (c) without resonators and (d) with resonators.

Table 5.2: Design parameters of slit and hexagonal split ring slot (HSRS)

Parameter	Value (mm)	Parameter	Value (mm)
s1	1.5	p1	3.6
s2	8.5	p2	2.75
s3	4.6	t	0.9
t1	0.4		

The geometry and prototype of proposed broadband MIMO antenna are shown in Figure 5.4. It is composed of two identical castor leaf-shaped QSCAs having smooth corners, which are arranged in mirror-image configuration to each other. Owing to this arrangement, the impedances seen by excitation ports of both antenna elements are identical and the direction of radiation is oppositely oriented with respect to one another when port 1/2 is excited and port 2/1 is matched terminated one after another. For higher isolation in lower frequency range, the distance between antenna elements is increased by 2 mm. The overall size of the proposed MIMO antenna is 66.8×40×0.8 mm^3. It was designed using FR4 substrate explained earlier.

Further, each radiating patch is loaded with two resonators: a slit and a hexagonal split ring slot (HSRS) as shown in Figure 5.4. The slit and the hexagonal split ring slot are formed for elimination of overlapping WiMAX and WLAN communication bands respectively. The point Xr (0 mm, 0 mm , 0 mm) is taken as reference point to define the centre point Yr (-3.8 mm, 9.5 mm, 0 mm) of HSRS and starting point Zr(0 mm, 25 mm, 0 mm) of the slit. The HSRS is advantageous for the proposed antenna having distinct segments over conventional rectangular split ring slot (RSRS) [Gao *et al.* (2014)]. In the present case, HSRS is placed in such a manner that it stops the current flow along the patch boundary as shown in Figures 5.5 and 5.10. Also, the space required for creating RSRS in the antenna structure is more than that required for creating HSRS to couple energy from the slit to the slot which would disturb the surface current distribution around the slit to obtain WiMAX band-notch. The quarter guide wavelength slit and half guide wavelength HSRS act as resonators at corresponding frequencies. These resonators provide anti-resonance for the antenna at the respective notch frequencies. The procedure for design of resonators in the frequency bands to be rejected can be explained with the help of vector surface current distributions around the boundaries of resonators. Figure 5.5 shows the enlarged view of vector current distribution on the surface of patch. It can be clearly investigated from Figure 5.5 that the slit outer boundary accommodates one half-wavelength at 3.5 GHz whereas the HSRS outer

boundary accommodates two half-wavelengths at 5.5 GHz. Each half-wavelength variation of current is shown by solid lines around the boundaries of resonators at the corresponding frequencies. By applying the foregoing concept, the lengths of slit ($L_{3.5}$) and slot ($L_{5.5}$) can be deduced by equations (5.1) and (5.2) given below.

$$L_{3.5} = s1 + s2 + s3 + t1 \approx 0.29\,\lambda g \tag{5.1}$$

$$L_{5.5} = 2 \times p1 + 4 \times p2 - t \approx 0.52\,\lambda g \tag{5.2}$$

$$\lambda g = \frac{c}{f_r \sqrt{\varepsilon_{eff}}} \tag{5.3}$$

$$\varepsilon_{eff} = \frac{\varepsilon_r + 1}{2} \tag{5.4}$$

where c is the speed of light, f_r is the center frequency of the band to be rejected, λ_g is the guide wavelength, ε_{eff} is the effective relative permittivity, and ε_r is relative permittivity of the substrate as mentioned in reference [Gao *et al.* (2014)].

It is found from equations (5.1) and (5.2) that the lengths of slit and slot are about one-quarter and one-half guide wavelengths respectively at the corresponding notch frequencies as mentioned in references [Zhu *et al.* (2016) and Gao *et al.* (2014)]. In other words, length of each resonator is half of its outer boundary dimension in terms of wavelength at the corresponding notch frequencies as observed from Figure 5.5.

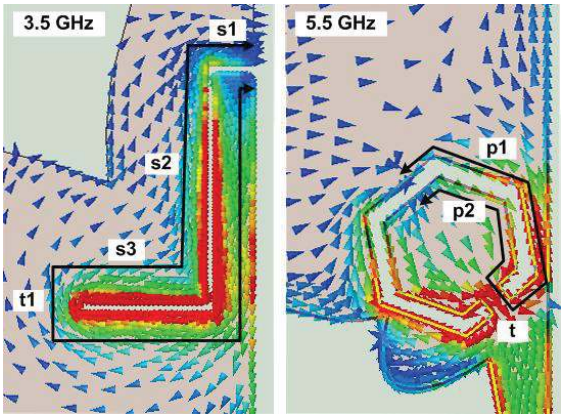

Figure 5.5: Vector surface current distributions on the proposed antenna patch at 3.5 and 5.5 GHz for deducing resonators' lengths.

The effects of resonator dimensions on S_{11}-frequency characteristic of the MIMO antenna are explained through parametric study. The optimized dimensions of resonators are listed in Table 5.2.

5.4 Simulation and Measurement of Castor Leaf-shaped MIMO Antennas

5.4.1 *Simulation Study*

The design and simulation of single element castor leaf-shaped quasi-self-complementary antenna and its MIMO configurations were performed using computer simulation technology microwave studio (CST MWS) software. The optimum dimensions of the MIMO antenna were found by optimizing all the design parameters which are listed in Tables 5.1 and 5.2. The MIMO antennas without and with resonators having optimum dimensions were then used to obtain simulated input and far-field characteristics including S-parameter-frequency characteristics, surface current distributions, co-polar radiation patterns in principal planes, variations of gain, total radiation efficiency and envelope correlation coefficient (ECC) with frequency.

5.4.2 *Parametric Study*

The dimensions of resonator parameters were adjusted to obtain proper centre frequencies and bandwidths of the frequency bands to be rejected. To better understand the effects of changes in resonator parameters, one parameter was varied at a time while other parameters were kept constant. The corresponding results are presented in terms of simulated reflection coefficient (S_{11})-frequency characteristics of the proposed antenna.

Figure 5.6 presents the effects of design parameters (s1, s2, s3 and t1) of slit (responsible for rejection of WiMAX band) on S_{11}-frequency characteristic of the MIMO antenna. It is observed from Figure 5.6(a) that the lower edge as well as the centre frequency of the frequency band to be rejected decrease when length ‘s1’ increases and the optimum bandwidth for rejected band is obtained for s1 = 1.5 mm. Similarly with the increase in length ‘s2’ of the slit, the centre frequency as well as the rejected band shifts towards lower frequency side without affecting

the bandwidth, and the optimum band rejection is obtained for s2 = 8.5 mm as shown in Figure 5.6(b). The increase of length 's3' of the slit decreases the lower edge frequency as well as the centre frequency of the rejected band, and the optimum value of 's3' is 4.6 mm as observed from Figure 5.6(c). The effect of variation of slit width 't1' is shown in Figure 5.6(d), which depicts that increase of width 't1' increases the bandwidth as well as higher edge frequency of rejected band, and the optimum bandwidth is found for t1 = 0.4 mm. The decrease of notch frequency with increase in lengths 's1', 's2' and 's3' of the slit is obtained due to increase of slit length $L_{3.5}$ (= s1+s2+s3+t1). In addition, these parameters do not have significant effect on WLAN band to be rejected.

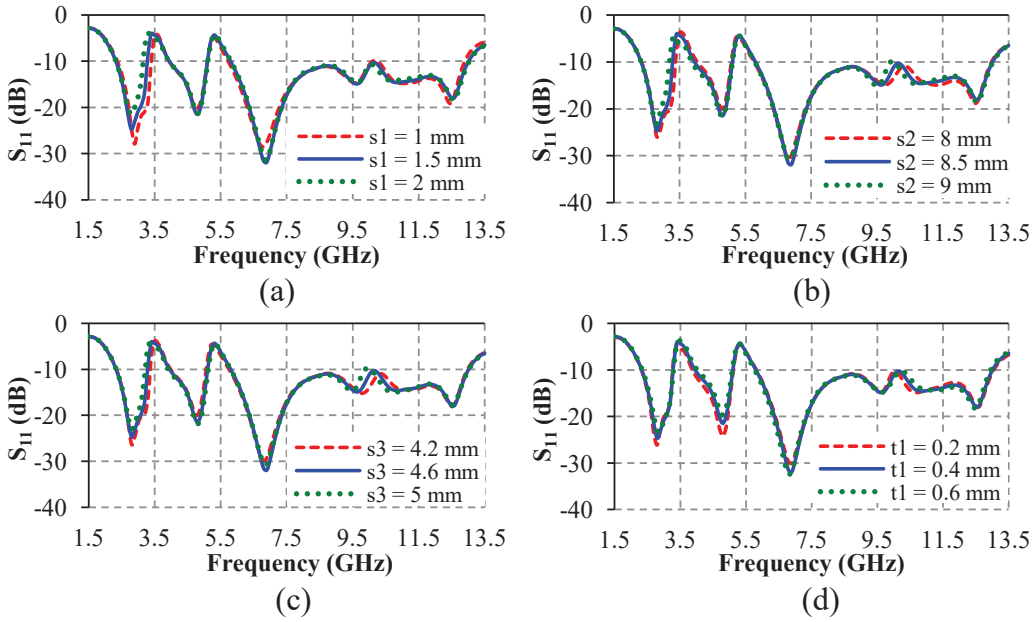

Figure 5.6: Variations of S_{11}-frequency characteristics of the MIMO antenna with slit parameter (a) s1, (b) s2, (c) s3, and (d) t1.

The effects of design parameters ('p1', 'p2' and 't') of HSRS responsible for WLAN band rejection on S_{11}-frequency characteristic of the antenna are shown in Figure 5.7. It is observed from Figure 5.7(a) that the centre frequency and the frequency band of WLAN band to be rejected shifts towards lower frequency side and corresponding bandwidth increases with increase in HSRS length 'p1'. The optimum bandwidth is found for p1 = 3.6 mm. The increase in HSRS length 'p1' simultaneously increases HSRS length $L_{5.5}$ (= 2×p1+4×p2−t)

and width of slot which simultaneously decreases the centre frequency and increases the bandwidth of WLAN band to be rejected. Similarly, Figure 5.7(b) shows that the centre frequency as well as whole WLAN band shifts towards lower frequency side with increase in HSRS length 'p2'. It is also due to the simultaneous increase in length '$L_{5.5}$' and hexagonal area surrounded by HSRS, and the optimum value of 'p2' is found to be 2.75 mm. Further, the effect of variation in gap 't' on the antenna characteristics is presented in Figure 5.7(c). It is observed from Figure 5.7(c) that WLAN band and its centre frequency increase with increase in the value of 't', because the increase in the gap 't' decreases the slot length '$L_{5.5}$'. It is also found that variation in the dimensions of HSRS has no effect on WiMAX band.

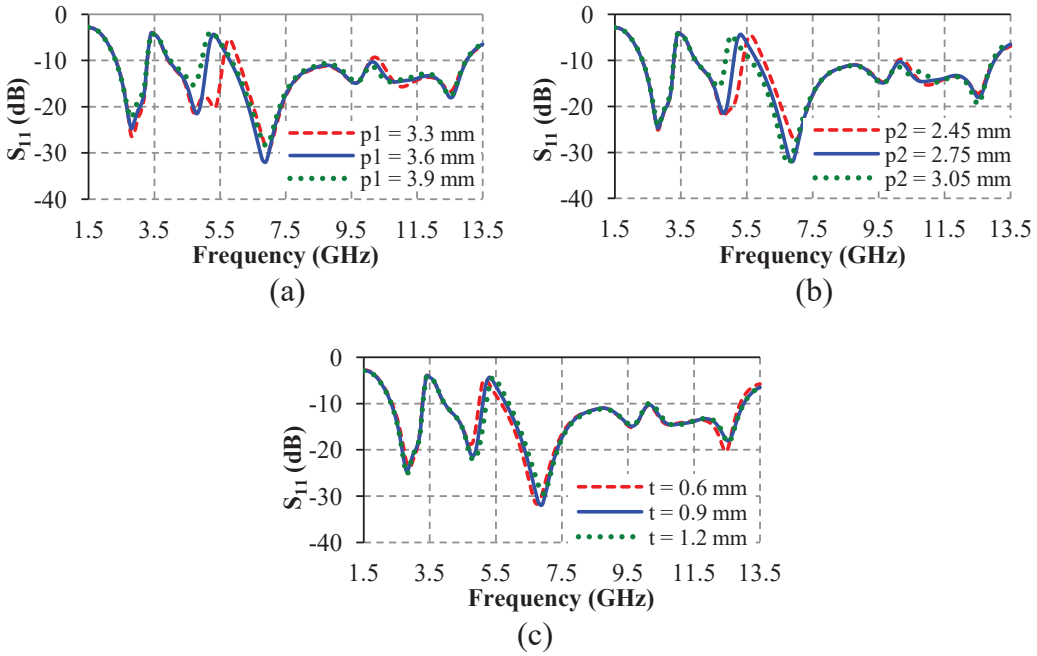

Figure 5.7: Variations of S_{11}-frequency characteristics of the antenna with HSRS parameter (a) p1, (b) p2, and (c) t.

To illustrate the influence of each resonator that provides band-rejection, the reflection coefficients (S_{11})-frequency characteristics of the MIMO antenna loaded with only slit, only HSRS and both slit and HSRS are shown in Figure 5.8.

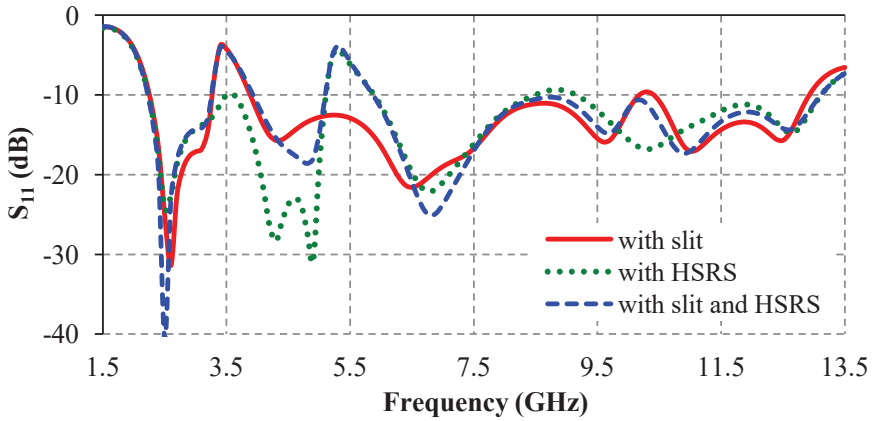

Figure 5.8: Variations of S_{11}-frequency characteristics of the antenna loaded with only slit, only HSRS, and both slit and HSRS.

It is clear from Figure 5.8 that S_{11} is greater than or equal to -10 dB for frequency range of 3.25−3.85 GHz when the patch is loaded with 0.29 λ_g long slit only. Similarly, when the patch is loaded with 0.52 λ_g long HSRS only, the frequency range for obtaining $S_{11} \geq$ -10 dB is 5.10−5.85 GHz. In addition, when the antenna is loaded with both slit and HSRS, the values of $S_{11} \geq$ -10 dB are obtained for frequency ranges of 3.25−3.85 GHz and 5.10−5.85 GHz. It indicates that both the interfering bands are rejected simultaneously when the patch is loaded with both slit and HSRS of proper dimensions

5.4.3 *Experimental Study*

After obtaining the optimum dimensions through simulation and parametric studies, the proposed MIMO antennas having two elements of castor leaf-shaped QSCAs without and with two resonators used for rejection of WiMAX and WLAN bands were fabricated. The single element as well as two-element MIMO antennas with and without the resonators having optimum dimensions are fabricated using LPKF PCB prototyping machine (Model: ProtoMat S103). The fabricated antennas were tested experimentally over the frequency range 1.5−13.5 GHz. The measurement procedures are similar to those for TTLPA (see Sub-section 3.2.3.2). The values of S-parameters over the frequency range 1.5−13.5 GHz were measured using Anritsu make VNA Master Vector Network Analyzer (Model No.: MS2038C). The co-polar radiation

patterns of the proposed MIMO antennas without and with resonators in E-plane (yz-plane) and H-plane (xz-plane) were measured in an anechoic chamber at the discrete frequencies of 4, 8 and 12 GHz using setups identical to those described in Sub-section 3.2.3.2. The experimental gain values were also determined experimentally at different frequencies using comparison method described in Sub-section 3.2.3.2.

In addition, measurement of total efficiency over the operating frequency band of the MIMO antenna without and with resonators was made using Wheeler cap method [Huynch (2014)]. A copper cylindrical box with a radius of $\lambda/2\pi$ at 1.5 GHz was used as the Wheeler cap. Copper tape with conductive adhesive was employed for proper grounding of the cap. The photograph of the experimental arrangement for measuring total efficiency of the proposed antennas is shown in Figure 5.9. Figure 5.9 shows the location of antenna and ground connection inside the cap before and after covering top portion of the Wheeler cap with copper sheet.

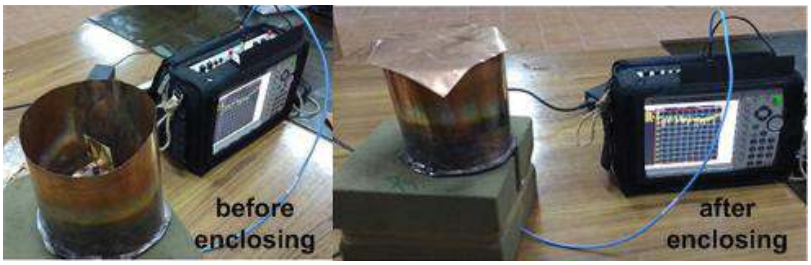

Figure 5.9: Experimental setup for measuring total efficiency of proposed antenna using Wheeler cap method.

The Wheeler cap was calibrated with the help of a wire half-wave dipole antenna designed at 2.1 GHz to authenticate the measurements made on the proposed antenna. The reflection coefficients at port 1 for each antenna were measured over the frequency range 1.5−13.5 GHz when the antenna was placed in free space and inside the Wheeler cap. The reflection coefficient measured at port 1 when antenna was kept in free space is 'S_{11FS}' whereas when antenna was kept inside the Wheeler cap is 'S_{11WC}'. The total efficiency (η_T) of the antennas without and with resonators is calculated using equation (5.5) given below.

$$\eta_T = (1 - |S_{11FS}|^2)\sqrt{\frac{|S_{11WC}|^2 - |S_{11FS}|^2}{1 - 2|S_{11FS}|^2 + |S_{11FS}|^2|S_{11WC}|^2}} \quad (5.5)$$

The simulated and corresponding measured results of the proposed antenna without and with resonators for S-parameters-frequency characteristics, 2D-radiation patterns, variations of gain and total efficiency with frequency were compared and discussed in different Sub-sections of Results and Discussion Section 5.4.

5.5 Results and Discussion

5.5.1 *S-parameters-Frequency Characteristics*

The impedances seen by the two excitation ports of proposed MIMO antenna are same due to the identical antenna elements arranged in mirror-image configuration, and hence $S_{11} = S_{22}$ and $S_{21} = S_{12}$. The simulation and experimental studies of S-parameter-frequency characteristics of both the MIMO antennas were carried out over the frequency range 1.5−13.5 GHz. The S-parameters of the antennas were measured using Anritsu make Vector Network Analyzer (Model: 2038C). Both simulated and measured results for variations in S_{11}- and S_{21}- values of the antennas with frequency are shown in Figure 5.10(a) and (b) respectively. It can be seen from Figure 5.10 that the trend of variation of simulated and measured results are nearly in agreement with each other. The antenna without resonators achieves simulated and experimental impedance bandwidth (for $S_{11} \leq$ -10 dB) of 5.95:1 (2.2−13.1 GHz) and 5:1 (2.6−13.0 GHz) respectively as shown in Figure 5.10(a). In addition, the presence of resonators on the antenna patches suppresses the frequency ranges of 3.25−3.85 GHz (WiMAX band) and 5.1−5.85 GHz (WLAN band) where the values of reflection coefficient 'S_{11}', are more than -10 dB as observed from both simulated and experimental S_{11} versus frequency curves of the antenna with resonators.

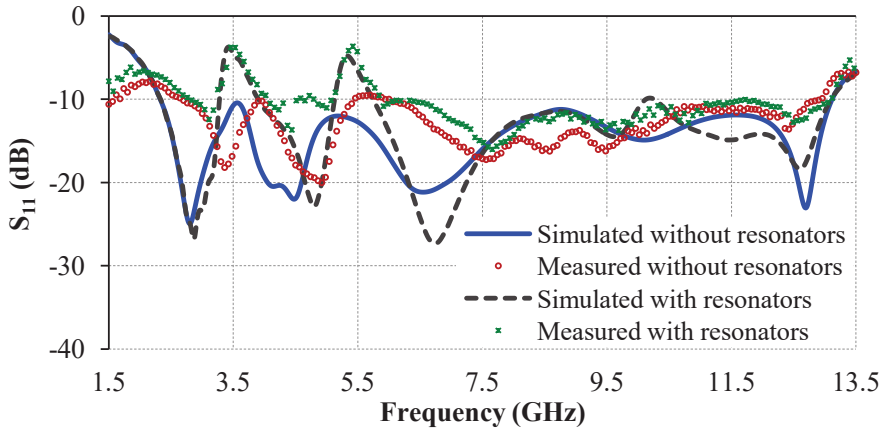

(a)

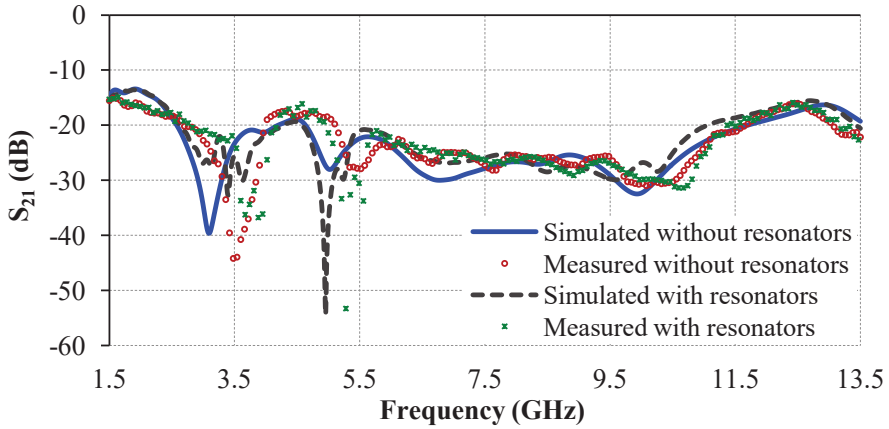

(b)

Figure 5.10: S-parameters-frequency characteristics of the proposed MIMO antenna (a) S_{11} and (b) S_{21}.

Further, it is seen from Figure 5.10(b) that the simulated and experimental values of S_{21} of both the antennas are less than -15 dB which indicates high isolation between antenna ports over its operating frequency range 2.2−13.1 GHz.

5.5.2 *Simulated Surface Current Distributions*

The simulation study of proposed MIMO antenna with and without resonators was also done in terms of current distribution on the surface of antenna at centre frequencies (3.5 and 5.5 GHz) of rejected frequency bands and at one higher frequency of 10 GHz, and the results are shown in Figure 5.11. Surface current distributions for the antenna with and without resonators were obtained when port 1 is excited and port 2 is terminated in 50 Ω load. This was done keeping in view the identical nature of antenna elements.

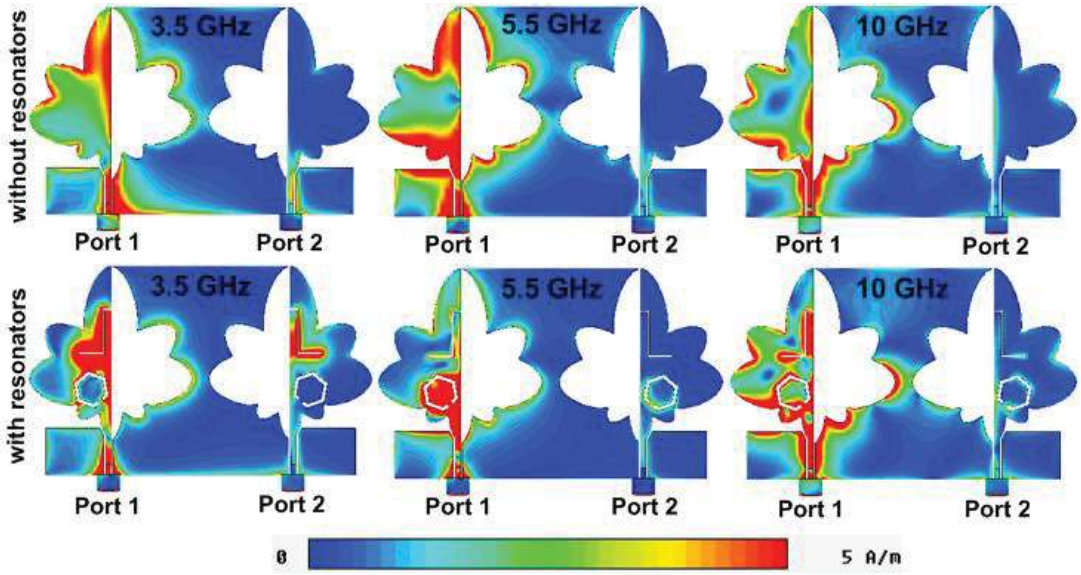

Figure 5.11: Simulated current distributions on the surface of the proposed MIMO antenna with port 1 excited and port 2 match-terminated.

It is easy to observe from Figure 5.11 that current is concentrated near the boundaries of radiating patch and complementary slot of the excited element of each antenna except for antenna with resonators at 3.5 and 5.5 GHz. The slit is placed in the upper part of patch where higher level of current is concentrated at 3.5 GHz as shown in excited element of antenna without resonators. Similarly higher level of current concentration is obtained in upper as well as lower parts of excited element of antenna without resonators for 5.5 GHz. The HSRS is positioned in lower part of patch because most of the lower patch region doesn't accommodate higher level of current at other frequencies except for 5.5 GHz. Due to the placement of these resonators, the current is concentrated around slit and hexagonal split ring slot (HSRS) resonators at 3.5 and 5.5 GHz respectively while it is distributed on almost the whole radiating patch of the antenna without resonators. It indicates that the concentration of surface current around these resonators restricts its flow around the antenna edges which stops the WiMAX (3.25−3.85 GHz) and WLAN (5.1−5.85 GHz) frequency bands from getting radiated by the antenna. Further, current concentrates not only around the resonators but also around the boundary of the excited patch of the antenna with resonators at 10 GHz which is similar to the current distributions around the

boundary of the excited patch of the antenna without resonators at same frequency.

In addition, it can be observed from the surface current distributions on the antenna without resonators that with increase in frequency, single current path is divided into parts providing maximum and minimum levels of current according to excitation frequency. This indicates that the patch and slot boundaries accommodate higher number of half-wavelength current paths as frequency increases. It can also be noticed that level of current density on feed line of element '2'of both antennas is lesser at the frequency of 10 GHz in comparison to the levels at 3.5 and 5.5 GHz. This indicates that the mutual coupling between antenna ports 1 and 2 is lesser at 10 GHz as compared to that at 3.5 and 5.5 GHz. It can also be verified from simulated S_{21}-frequency characteristics shown in Figure 5.10(b). Similar current distributions can be seen on the surface of antenna element '2' when exciting port 2 and keeping port 1 match-terminated.

5.5.3 *Radiation Patterns*

Due to the self-complementary structure, the antenna radiates more in the direction of radiating patch. It was verified through simulation study of three-dimensional (3D) far-field radiation patterns of both MIMO antennas when excitation is provided at port 1/2 while port 2/1 is match-terminated with 50 Ω load. The simulated 3D radiation patterns of the antennas for total gain at center frequency of 7.5 GHz are shown in Figure 5.12. It can be observed from Figure 5.12 that the radiation patterns of proposed MIMO antennas are oppositely oriented along yz-plane when element '1' is excited through port 1 and element '2' is terminated in 50 Ω load using port 2 and vice-versa. This indicates that radiation patterns of the antenna elements are mirror-images of each other in yz-plane and hence good pattern diversity can be achieved through the proposed MIMO antennas.

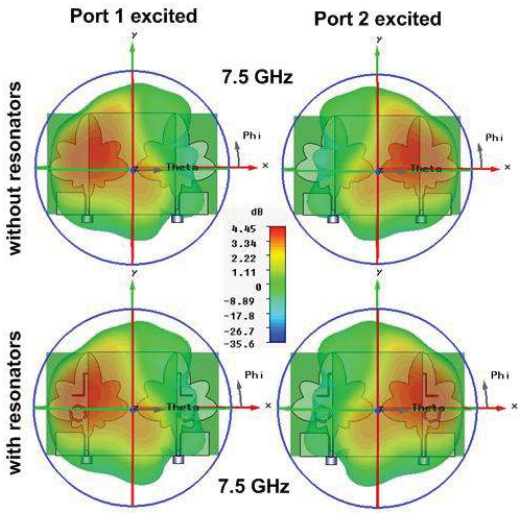

Figure 5.12: 3D radiation patterns of the proposed MIMO antenna when port 1/2 is excited while port 2/1 is match-terminated.

Further, due to the mirror-image nature of radiation patterns, two-dimensional (2D) radiation patterns of the antenna with only one port excited and other match-terminated are discussed. The simulated and measured 2D radiation patterns (for power) normalized with respect to maximum power in H- and E-planes of the MIMO antennas with port 1 excited and port 2 terminated with 50 Ω load at 4, 8 and 12 GHz are shown in Figure 5.13. Figure 5.13 shows that the simulated 2D radiation patterns of both the antennas at different frequencies over the operating frequency range are nearly in agreement with respective experimental patterns. It can also be observed from Figure 5.13 that the radiation patterns in H (xz)-plane are quasi-omnidirectional at 4, 8 and 12 GHz, and quite directional around an angle of 270^0 at 4 and 12 GHz. At 8 GHz, it is quite directional around angles 210^0 (and 330^0). This quite directional radiation along the excited element (placed along negative x-axis or 270^0 in H-plane) is obtained probably due to the radiation from distinct segments of excited element at different frequencies. In E (yz)-plane, radiation patterns are different from 'dumb-bell' shape but slightly directional around 90^0 (direction of tip of castor leaf) and less radiation around 270^0 (direction of feed and ports) at 4, 8 and 12 GHz. It is also noticed from 2D patterns that number of side lobes increases with increase in frequency. It may due to the generation of higher order modes with increasing frequency.

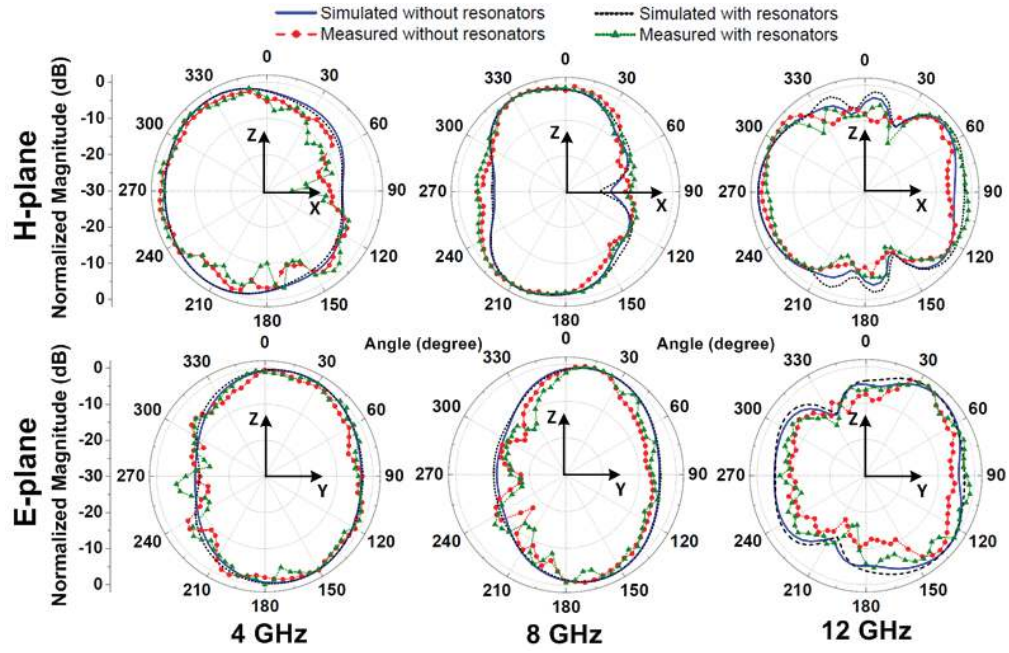

Figure 5.13: 2D radiation patterns of the proposed MIMO antenna when port 1 excited and port 2 match-terminated.

5.5.4 *Realized Gain- and Total Efficiency-Frequency Characteristics*

Figure 5.14 shows the variations of simulated and measured realized gain values of the proposed antennas in broadside direction without and with the resonators versus frequency with port 1 of each antenna excited and port 2 terminated in 50 Ω load. It is clear from Figure 5.14 that simulated gain values of both antennas are nearly in agreement with the respective experimental values over the operating frequency band of the antenna. Further, the simulated gain values of antenna without resonators vary in the range 0.76 (at 2 GHz) − 6.02 dBi (at 11 GHz) over the frequency range (1.5−13.5 GHz) while the experimental gain values vary from 2 dBi (at 2.5 GHz) to maximum of 6.10 dBi (at 10 GHz) over the frequency range of 2.5−12 GHz. It can also be noticed from Figure 5.14 that the simulated and experimental gain values of antenna with resonators lie in the range 1.68 dBi (at 2.2 GHz) − 6 dBi (at 9.5 GHz) over the simulation frequency range, and 2.5 dBi (at 2.5 GHz) − 5.7 dBi (at 9.5 GHz) over the experimental frequency range respectively, except over two stop bands about the frequencies of 3.4 and 5.3 GHz. The sharp decrease of antenna gain is obtained at frequencies where S_{11} (≈ -4 dB) is maximum.

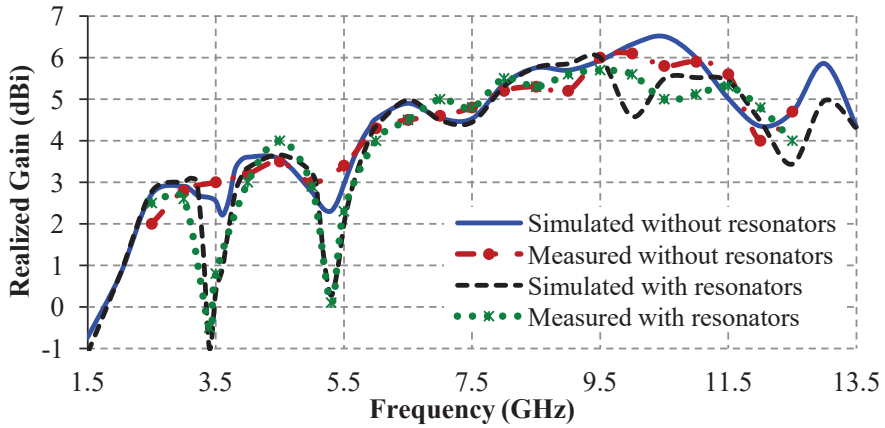

Figure 5.14: Realized gain-frequency characteristics of the proposed MIMO antenna.

Further, variations of simulated and measured total efficiency (η_T) of both the antennas with frequency are compared in Figure 5.15. It is observed from Figure 5.15 that the simulated values of total efficiency (η_T) are more than 80 % over the whole operating frequency range for the antenna without resonators while the antenna with resonators radiates with more than 75 % efficiency, except over two stop-bands. The measured values of total efficiency (η_T) for both the antennas vary between 70−90 % up to 7.5 GHz except over two stop-bands whereas the parameter values vary in the range 60−70 % in higher frequency range (more than 7.5 GHz). The deviation between measured and simulated total efficiency values over the operating frequency range of the antennas may be due to fabrication and experimental errors as well as bigger electrical size of the cap at higher frequencies. Both gain and total efficiency of antenna with resonators decrease significantly at stop-band frequencies of 3.4 and 5.3 GHz when compared with antenna without resonators, which demonstrates the effective band-rejection capability of the resonator-antenna combination. In addition, it is observed that with increase in frequency, gain increases while total efficiency decreases for both the antennas. The trend of variation of gain with frequency may be due to increase in antenna dimensions in terms of wavelength as frequency increases. The decrease of total efficiency with increase in frequency may be due to increase in substrate losses with frequency. The effect of changes in substrate parameters with frequency on antenna performance would be similar to that discussed in sub-section 4.3.3.6 of chapter 4.

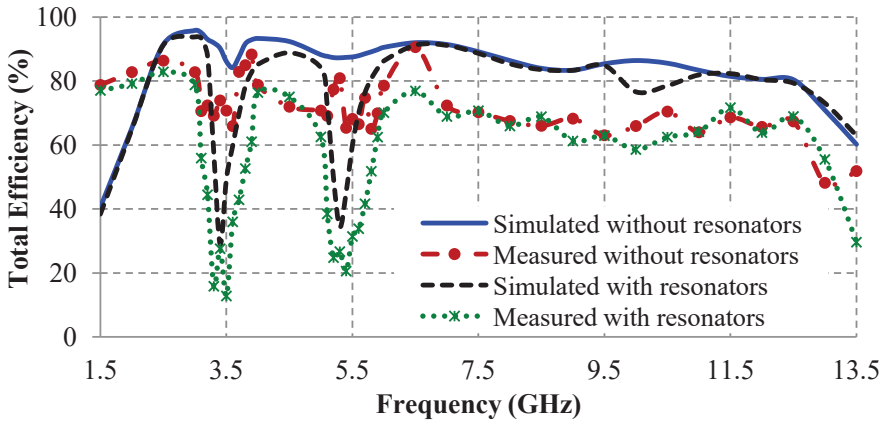

Figure 5.15: Total efficiency-frequency characteristics of proposed MIMO antenna.

5.5.5 *Envelope Correlation Coefficient*

One of the key parameters of MIMO antenna is correlation between antenna elements called envelope correlation coefficient (ECC), which describes its diversity performance. It should be as low as possible and can be evaluated using S-parameters [Blanch *et al.* (2003)]. In the present study, ECC was computed using its relation with S-parameters given below.

$$ECC = \frac{|S_{11}^{*}S_{12}+S_{21}^{*}S_{22}|^{2}}{(1-(|S_{11}|^{2}+|S_{21}|^{2}))(1-(|S_{22}|^{2}+|S_{12}|^{2}))} \tag{5.6}$$

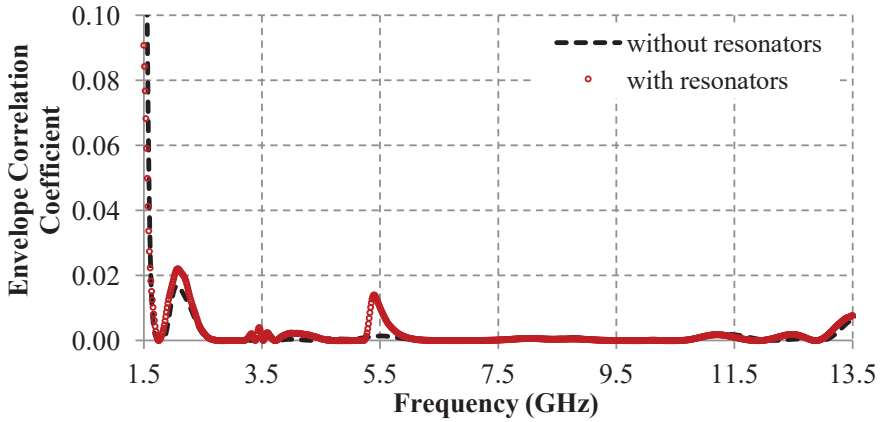

Figure 5.16: Variations of envelope correlation coefficients of the proposed MIMO antenna with frequency.

The variations of simulated values of ECC between the antenna elements of both MIMO antennas with frequency are shown in Figure 5.16. It is seen from Figure 5.16 that ECC values for both MIMO antennas are less than 0.02 (well

below the allowed limit of ECC = 0.1) for the whole operating frequency range. The low values of ECC indicate that the proposed antennas with and without resonators have the capability of providing very good diversity performance.

5.6 Summary

In this chapter, simulation and experimental studies of single-sided MIMO antennas with and without dual band-rejection characteristics using two-elements of castor leaf-shaped QSCA with smooth corners have been reported. The simulated and measured characteristics of the antennas are nearly in agreement with each other. The QSCA with smooth corners has been found to be more compact in size as compared with QSCA with sharp corners while the lower cutoff frequency for both QSCAs is the same. The simulated reflection coefficient-frequency characteristic of single element QSCA with smooth corners has also been compared with corresponding measured results. The proposed two-element MIMO antenna has been found to provide broad impedance bandwidth of 10.9 GHz (2.2−13.1 GHz), which covers entire UWB along with Bluetooth frequency spectrum. The WiMAX and WLAN communication bands interfering with UWB are rejected using slit and hexagonal split ring slot resonators loaded on the radiating patch of the antenna. The antennas achieve good gain, total efficiency and very good diversity performance over the frequency band of interest. High isolation has been achieved between the elements of MIMO antennas without using any extra isolation technique. These inherent properties demonstrate that the presented MIMO antenna with dual band-rejection characteristics can be a promising candidate for broadband diversity applications and devices which require UWB along with Bluetooth frequency spectrums.

After investigations on castor leaf-shaped QSCA and discussion of its suitability as a MIMO antenna element in the present chapter, a broadband MIMO antenna using shared radiator is taken up for investigation in the next chapter.